Computers and Concrete, *Vol. 23, No. 6 (2019) 399-408*
DOI: https://doi.org/10.12989/cac.2019.23.6.399

Theoretical and experimental investigation of piezoresistivity of brass fiber reinforced concrete

Aurore Mugisha[1a] and Egemen Teomete[*2]

[1]*The Graduate School of Natural and Applied Sciences, Dokuz Eylül University, Izmir, Turkey*
[2]*Civil Engineering Department, Dokuz Eylül University, Kaynaklar, Buca, Izmir, Turkey*

(Received January 28, 2019, Revised March 29, 2019, Accepted April 22, 2019)

Abstract. Structural health monitoring is important for the safety of lives and asset management. In this study, numerical models were developed for the piezoresistive behavior of smart concrete based on finite element (FE) method. Finite element models were calibrated with experimental data collected from compression test. The compression test was performed on smart concrete cube specimens with 75 mm dimensions. Smart concrete was made of cement CEM II 42.5 R, silica fume, fine and coarse crushed limestone aggregates, brass fibers and plasticizer. During the compression test, electrical resistance change and compressive strain measurements were conducted simultaneously. Smart concrete had a strong linear relationship between strain and electrical resistance change due to its piezoresistive function. The piezoresistivity of the smart concrete was modeled by FE method. Twenty-noded solid brick elements were used to model the smart concrete specimens in the finite element platform of Ansys. The numerical results were determined for strain induced resistivity change. The electrical resistivity of simulated smart concrete decreased with applied strain, as found in experimental investigation. The numerical findings are in good agreement with the experimental results.

Keywords: finite element model; smart concrete; strain; electrical resistivity; piezoresistivity; self-sensing; smart material; structural health monitor

1. Introduction

Earthquakes, material deteriorations and other environmental factors challenge the concrete structures. Structural health monitoring is important for safety of lives and asset management. Structural health monitoring systems have gradually become a technique deployed to assess the performance of concrete structures and to program maintenance and repair work in a more economical way. The structural condition or health of concrete structures during service life can be monitored considering various parameters including strain (or deformation), stress (or force), crack, damage, temperature and humidity. The conventional metal foil strain gages used for structural health monitoring can get point wise measurement. Consequently, they have to be used in large amounts. Chung (2002) stated that they are more expensive, less durable and have lower sensitivity than cement based composites.

A new concept of smart or self-sensing cement composite has been introduced (Baeza *et al*. 2011, Chen and Chung 1993, Han *et al*. 2015, Kamila 2013). It involves the ability of mortar to sense its own strain due to the effect of strain on the electrical resistivity (Baeza *et al*. 2011, Fu *et al*. 1997, Fu and Chung 1997, Wen and Chung 2000).

This electromechanical phenomenon is called piezoresistivity; it is achieved by mixing electrically conductive fillers such as steel fiber, short carbon fiber, carbon nanotube (CNT) and nickel powder into conventional mortar. It takes its origin from the slight fiber pull-out upon micro crack opening and the consequent loosening in fiber-matrix interface (Chung 2001, Wen and Chung 2006). It enables the use of electrical resistance measurement to detect the strain of cement composites. Baeza *et al*. (2011) tested cement paste samples with carbon fibers under compression test; four-wire measurement method was proposed; the effects of load value, load rate and humidity on strain sensitivity were reported and implementation of structural control system with smart composite was presented. The inclusion of conductive fibers to cement composites decreases its electrical resistance and application of loads affects electrical resistance (Teomete and Koçyigit 2015). The effect of crack length, thus damage, on the electrical resistivity of cement composites with steel and carbon fibers was investigated; strong linear relationship between crack length and electrical resistance change was reported (Teomete 2015, Teomete 2016, Teomete 2017). Tensile strain, which was applied by split tensile test, was found to be linearly correlated with electrical resistance change (Teomete and Koçyigit 2013). The effect of cross talk in which strain was perpendicular to electrical current in the cement composite was investigated and a phenomenological model of the effect was reported (Teomete 2014). Carbon fiber, carbon nanofiber (CNF) and carbon black (CB) reinforced multifunctional cementitious composites were investigated

*Corresponding author, Associate Professor
E-mail: egemen.teomete@deu.edu.tr, eteomete@gmail.com
[a]M.Sc.
E-mail: auroremugisha@gmail.com

ISSN: 1598-8198 (Print), 1598-818X (Online)

for strain sensing capability (Wang *et al.* 2018a, Wang *et al.* 2018b, Wang *et al.* 2018c, Li *et al.* 2006, Li *et al.* 2008, Chen and Liu 2008, Xiao *et al.* 2010, Azhari and Banthia 2017, Reza *et al* 2003).

Modeling of piezoresistivity of cement based composites was studied in the literature. A micromechanics model was developed to predict the piezoresistive properties of carbon nanotube cement-based nanocomposites and numerical simulations were compared to experimental results (García-Macías *et al.* 2017). Their conclusions highlighted that the strain-sensing capabilities of the cement-based nanocomposites was due to strain-induced changes in the volume fraction, filler orientation and changes in the tunneling resistance. García-Macías *et al.* (2018a) stated that there were two mechanisms in conductivity of CNT composites; electron hopping and conductive networking while the origins of the piezoresistivity were "a) strain-induced changes in the volume fraction b) changes in the conductive networks due to filler reorientation c) changes in the tunneling resistance through variation of the interparticle properties". Three independent piezoresistive coefficients were found to be necessary to fully define the piezoresistivity matrix. Finite element model of piezoresistivity of CNT reinforced cement composite was developed and tested for various 3D stress states for strain sensitivity. García-Macías *et al.* (2018a) determined that, transverse sensitivity was a little higher with respect to the longitudinal sensitivity; shear strain sensitivity of CNT reinforced cement composite was weak and smart concrete strain sensing ability can be modeled with one piezoresistive coefficient. García-Macías *et al.* (2018b) developed Euler-Bernoulli finite element models of beams with multiwall carbon nano tube (MWCNT) reinforced epoxy composite and used for 2D beam with multiple prescribed crack damages, and a 3D RC beam under four-point flexure. MWCNT/strips with full penetration electrodes were capable of sensing curvature, strain, discrete and smeared cracks of the concrete beam. García-Macías *et al.* (2018c) studied finite element model of beams with MWCNT reinforced epoxy strips for buckling detection. Smart composites with filler contents just above the percolation threshold gave linear response to strain. The smart MWCNT/epoxy composites increased the buckling load of the beams while they acted as buckling sensors. Parametric study results about filler content, boundary conditions and electrode layout were presented. Garcia- Macias and Ubertini (2019) investigated use of smart brick for strain and damage assessment of masonry structures under seismic loads by using finite element modeling. They determined that, electrically isolated bricks were more sensitive to strain with respect to unisolated bricks; smart bricks can be used to monitor the strain fields of existing and new masonry structures; Kriging reconstruction was used to interpolate strain fields between the sensor bricks. Damage detection and localization was achieved by merging strain and strain redistribution indexes which was obtained from electrical resistance change of smart bricks. Chowdhury (2017) investigated and modeled the strain sensing capability of two matrices containing metallic inclusions, portland cement matrix and iron-based carbonate binder matrix. Portland cement matrix contained four different iron replacement percentages by volume (10%, 20%, 30% and 40 %). The simulation was based on finite element analysis. The results showed that the model results comply with the experimental values. The resistivity increased with increasing load for both matrices and the strain sensing response increased with increase in iron percentage.

Table 1 The mass of the materials used in $1m^3$ concrete mix

Components	Mass (kg) in $1m^3$ Concrete
Brass fiber	70
Cement CEM II	499
Gravel 5-15 mm	539
Sand 0-5 mm	808
Silica fume	55
Water	205
Plasticizer	6

2. Experimental Work

The smart concrete mixture was made of cement CEM II, fine and coarse crushed limestone aggregates, silica fume, super-plasticizer SikaVisco High Tech 30 and short brass fibers. Brass fiber, which had a length of 1.5 mm and a diameter of 0.5 mm, was used at 0.8% by volume in the mix. The mass ratio of brass fiber to cement was 14%. The water/cement ratio was 0.41 after moisture adjustment in the aggregates. The amount of material used in $1m^3$ of smart concrete is presented in Table 1.

Smart concrete cube specimens with size of 75 mm were prepared. Embedded electrode configuration was adopted during the test. Pure copper wire mesh which had a mesh opening of 5mm and wire diameter of 600 µm was used as electrode because of its high electrical conductivity. The wire meshes were placed in molds prior to casting. The mix was cast in the molds and the specimens were removed from the mold 24 hours after casting and cured in water for 28 days.

Polarization due to DC current changes electrical resistance of cement matrix composites. In order to eliminate polarization effects on the electrical resistance, 20 V DC current was supplied to the samples just before compression tests and the electrical resistance was monitored. When the electrical resistance reached steady state condition (which took approximately 15 minutes), the compression test was conducted so that the variation of electrical resistance during compression test was due to only strain.

Compression test was conducted in order to determine the electrical resistivity change (%ρ)-strain relationship of the specimens. Prior to loading, two strain gages were attached on the specimens to monitor the strain as illustrated in Fig. 1(a). Glass fiber epoxy composite plates were used to provide electrical insulation between the loading heads and the specimens as shown in Fig. 1(b). The test was performed using a Shimadzu AGS-X mechanical test machine of 300 kN frame capacity at a rate of 0.5 $mm.min^{-1}$ according to ASTM C39 standard.

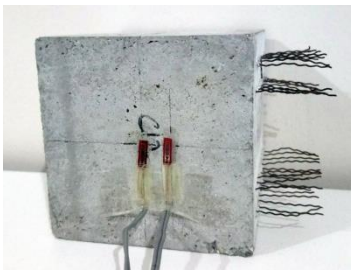

(a) the specimen

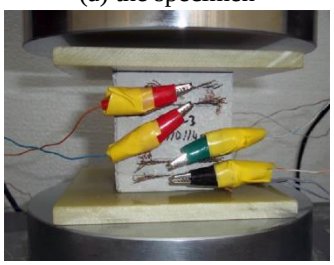

(b) the specimen at test

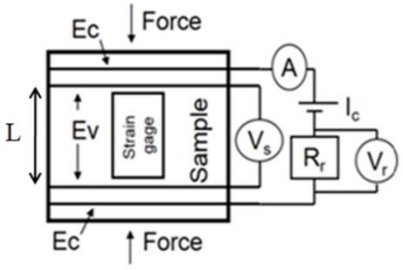

(c) the test circuit

Fig. 1 Compression test of smart concrete

During loading, current supply and voltage measurement were achieved using four electrode method: 20V DC current was supplied through one pair of outer electrodes (*Ec*), while the potential difference across the sample (*Vs*) was measured using a different pair of inner electrodes (*Ev*) as in Fig. 1(c). Distance between electrodes and sample cross section do not affect the four electrode method (Chiarello and Zinno 2005, Han *et al*. 2007).The sample was in series with a shunt resistance *Rr*=1000Ω. The potential difference across the shunt resistance was measured as *Vr*. The current *Ic* was measured during the test using a Digital Multimeter (A) which was in series with the circuit.

The voltages *Vs* and *Vr*, the strain gage data, the electric current (*Ic*), the load and the stroke of the loading head were recorded at a rate of 10 Hz (10 data in a second) using a National Instruments data logger.

The electrical resistance of a specimen (*Rs*) at any time of the test was determined by Ohm's Law as

$$R_s = V_s / I_c \tag{1}$$

The electrical resistivity ρ and the percent change in the electrical resistivity of the specimen % ρ were respectively determined as

$$\rho = (R \times A)/L \tag{2}$$

$$\%\rho = (\rho / \rho_0 - 1) \times 100 \tag{3}$$

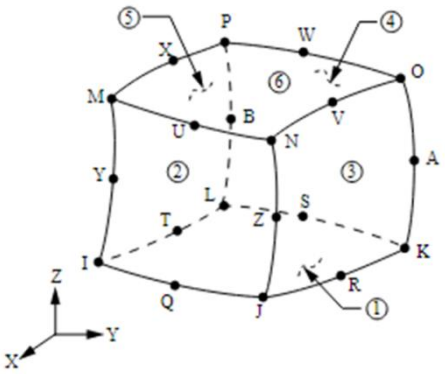

Fig. 2 SOLID226 Element's geometry, node locations and coordinate system in Ansys (2011)

where *R* is the electrical resistance of a specimen at any time of the test, *L* the gage length, (the length between the inner electrodes, which is equal to 0.035 m), A the cross-sectional area perpendicular to this length and ρ_o is the electrical resistivity of the specimen prior to loading.

3. Numerical model development

The compression tests conducted on the two specimens were modeled numerically using finite element program Ansys. To simulate the strain - electrical resistivity relation of smart concrete, two finite element models (FE-1and FE-2) were developed for the piezoresistive behavior of each smart concrete specimen. Piezoresistive static analysis was performed for each model.

SOLID226 element type was used to construct the model. The element is presented in Fig. 2. It has twenty nodes (illustrated by letters) with four degrees of freedom (DOFs) at each node: translations in the nodal *x*, *y* and *z* directions and voltage degree of freedom for electric conduction field. This translates to the capability of the solid element to model problems involving both structural and electrical properties of smart concrete.

In this study, numerical model of smart concrete was assumed to be isotropic and linear elastic. The element SOLID226 is capable of piezoresistive analyses, which was used for modeling smart concrete. The element's faces are illustrated by the circled numbers. Distributed surface loads, such as pressures, can be applied to the element's surfaces.

3.1 Material properties

SOLID226 element requires elastic constants, electrical resistivity and piezoresistive matrix to model a piezoresistive material. The material properties used in the analyses are given in Table 2.

Elastic constants include the modulus of elasticity of the tested smart concrete (*E*), and the Poisson's ratio (υ). The elastic modulus of the smart concrete specimens was determined experimentally by using the slope of the tangent to the stress-strain curve. It was equal to 38 GPa for both specimens. The Poisson's ratio was experimentally Table 2 The material properties for smart concrete

numerical models

FE Model	Young's Modulus E (GPa)	Poisson Ratio υ	Electrical Resistivity ρ_O (Ωm)	Piezoresistive Coefficients m_x, m_y, m_z
FE-1	38	0.18	356	51.79
FE-2	38	0.18	374	44.82

determined by strain measurements and was determined as 0.18.

In order to simulate the piezoresistive behavior of smart concrete, the electrical resistivity of tested specimens prior to loading (ρ_o) is required as input in the finite element model. ρ_o was determined using Eq. (2). In this equation, Ro corresponded to the electrical resistance of specimens at the beginning of the test.

For modeling of piezoresistive concrete, the piezoresistive matrix [m] is also required in finite element modeling. It is a 6×6 matrix that served to relate the *X*, *Y* and *Z* terms of normal strain to the corresponding terms of electrical resistivity change via 3 constants m_x, m_y and m_z as shown in the following equation

$$\begin{Bmatrix} \Delta\rho_x \\ \Delta\rho_y \\ \Delta\rho_z \\ \Delta\rho_{xy} \\ \Delta\rho_{yz} \\ \Delta\rho_{xz} \end{Bmatrix} = \begin{bmatrix} m_x & 0 & 0 & 0 & 0 & 0 \\ 0 & m_y & 0 & 0 & 0 & 0 \\ 0 & 0 & m_z & 0 & 0 & 0 \\ 0 & 0 & 0 & 0 & 0 & 0 \\ 0 & 0 & 0 & 0 & 0 & 0 \\ 0 & 0 & 0 & 0 & 0 & 0 \end{bmatrix} \times \begin{Bmatrix} \varepsilon_x \\ \varepsilon_y \\ \varepsilon_z \\ \gamma_{xy} \\ \gamma_{yz} \\ \gamma_{xz} \end{Bmatrix} \quad (4)$$

García-Macías (2018a) stated that cement based composite has low shear strain sensitivity while they can be modelled with one single piezoresistivity coefficient. Also, in our study, only uniaxial compression test was modelled, so, only longitudinal piezoresistive effect was considered in Eq. (4). For more information readers can refer to García-Macías (2018a).

Eq. (4) can be written in a compact form as

$$\{\Delta\rho\} = [m]\{\varepsilon\} \quad (5)$$

in which $\{\Delta\rho\}$ denotes the vector of change in electrical resistivity and $\{\varepsilon\}$ is the elastic strain vector with normal strain components (ε_x, ε_y, ε_z) and shear strain components (γ_{xy}, γ_{yz}, γ_{xz}).

In [m] matrix, the m_x, m_y and m_z piezoresistive coefficients express the relative change in resistivity due to normal strain. The *X*, *Y* and *Z* subscripts refer to the change in resistivity in one direction (*X*, *Y* or *Z* direction) caused by the applied strain in the same direction (*X*, *Y* or *Z* direction). These coefficients were obtained from the strain sensitivity data of the smart concrete specimen obtained from compression test. The strain sensitivity is the change in electrical resistivity per unit strain.

3.2 Geometry

The geometrical representation of the physical system is referred to as the solid model. The created solid model must be discretized in terms of nodes and elements in order to generate a finite element mesh and ultimately apply finite element analysis. There are two main ways offered in modeling the geometry part: (1) solid modeling and meshing, (2) direct generation. Solid modeling allows the user to create the geometric boundaries of the model, such as lines, areas or volumes and to control the size and shape of finite elements, then the meshing process is accomplished by using an automated finite element mesh operator. By contrast, in direct generation method, the coordinates of every single node and the size, shape, and connectivity of every single element are determined prior to defining these entities in the finite element model. Direct generation is more convenient for small or simple models than is solid modeling. However, for ease of modeling of three-dimensional models, solid modeling method was preferred in this study.

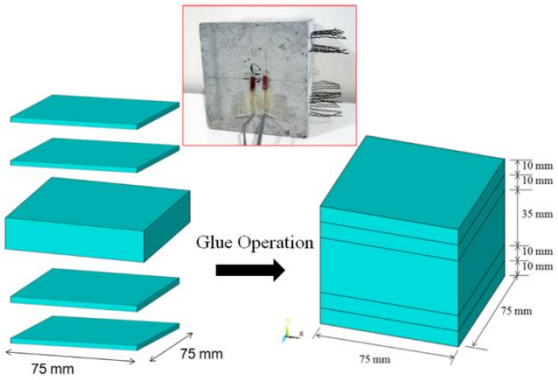

Fig. 3 Smart concrete solid model before and after glue operation

The cube model was 0.075m long with a cross-section of 0.075×0.075 m. The dimensions were input in meter (m). During creation of the geometry, each solid model was first formulated as 5 distinct rectangular blocks (as seen in Fig. 3); the lines separating adjacent blocks served as location of electrodes. An individual block was 0.075 m long. The middle block lying between the inner two electrodes had a height (*Ev*) of 0.035 m; its height symbolizes the gage length of the specimen. The 4 remaining blocks had a height of 0.010 m; their height illustrates the distance between inner and outer electrodes. All the 5 blocks were later combined using the glue operation. Glue operation is a Boolean operation available in ANSYS and useful to connect solid model entities that are touching one another but not sharing any part. At the end of the operation, no additional block was created but new parts that have one lower dimensionality (i.e., areas of intersection between adjacent blocks) were produced. Fig. 3 depicts a typical whole size solid model of smart concrete before and after glue operation, with intersecting lines representing the position of inner and outer electrodes.

3.3 Meshing

After establishing material properties and building the solid model, meshing was performed. The target was to work with the minimum number of elements for computational efficiency.

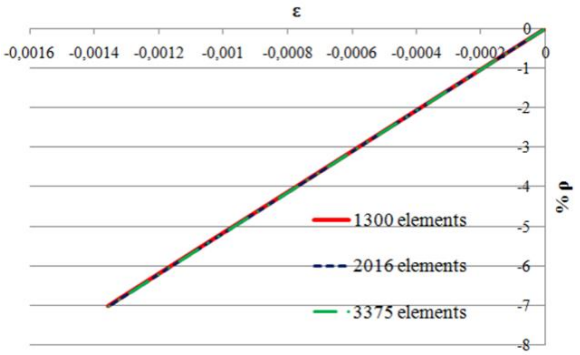

Fig. 4 (a) The % ρ - strain graph for three different element numbers

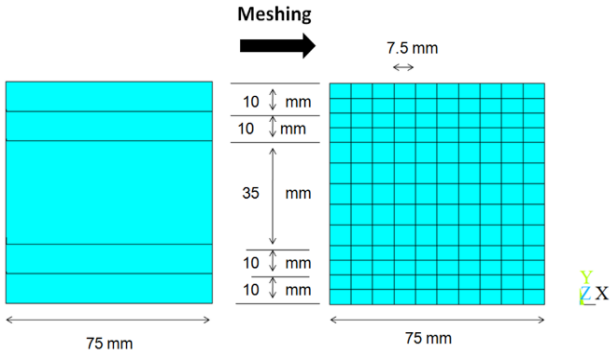

(b)

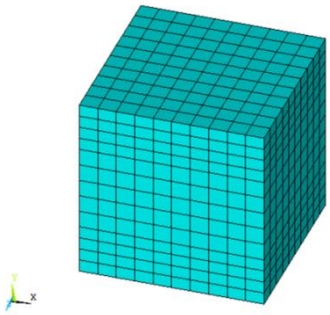

(c)

Fig. 4 The finite element mesh of smart concrete model in (b) XY plane (c) in XYZ space

Number of elements 1300, 2016 and 3375 were used to determine the mesh size for piezoresistive analyses. As can be seen in Fig. 4(a), the strain- electrical resistance graphs were very close for three different element numbers. For computational efficiency, minimum number of elements of 1300 were used for the analyses.

In this study, 20-node hexahedral (brick) coupled-field solid elements SOLID226 were used. They had 0.0075 m size each. Fig. 4(b) illustrates the result of the meshing operation of the solid model in XY plane: 10 elements along lines on the length and width of the model were produced; 13 elements were created by the height of the model, i.e., 5 elements along the height (0.035 m) of the middle volume which lies between two inner electrodes and 8 elements along the height (0.010 m) of the remaining 4 volumes. Fig. 4(c) shows the overall mesh, which comprises 1300 elements and 6347 nodes.

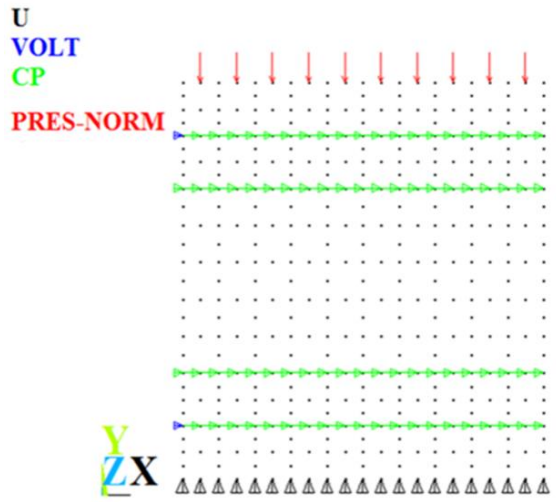

Fig. 5 The loading conditions of a finite element model in XY Plane, with vertical displacement constraint (U), coupled (CP) voltage constraints (VOLT) at electrodes, and distributed load pressure (PRES-NORM)

3.4 Loading

The word "loads" in Ansys terminology includes boundary conditions and externally or internally applied forces. The present problem requires application of displacement and voltage boundary conditions to the finite element (FE) model in order to simulate the actual structural support system and the current supply through electrodes. The pressure applied on the specimen can also be modeled in the form of distributed loads applied either on the solid model (areas) or on the finite element model (nodes located on areas).

In this study, the FE models were restrained vertically (in *Y* direction) at the bottom and were free in the horizontal (*X* and *Z*) directions, as the samples were tested experimentally. Fig. 5 shows the vertical constraints at the bottom of the numerical model, with UY (displacement translation in *Y* direction) equal to zero.

Nodal pressure was applied on top nodes, i.e., nodes located at *Y*=0.075 m. Nodal pressure is illustrated with red arrows in Fig. 5. The Ansys convention for pressure loading is that a positive load value represents pressure into the surface (compressive). The unit of pressure adopted throughout the modeling was Pascal (Pa).

Nodal pressure and electrical impulse were applied simultaneously on the models as it was during test. Due to electrical potential drop observed during test, 20V DC current was decreased by the shunt potential difference (*Vr*). The current was supplied through outer nodes located on supply electrodes by coupling VOLT degree of freedom. Coupling (CP) is essential if a particular DOF is expected to have the same value at several nodes (Madenci and Güven 2006). The nodes occupying the place of inner electrodes were also coupled in VOLT DOF in order to further determine the output potential difference across the FE model. In Fig. 5, the black dots represent the nodes of the FE model viewed in XY plane. The electrodes are shown by coupled set of nodes in green.

Table 3 The details of numerical methods used in finite element analyses

Numerical Method	Pressure Loads (MPa)
Single Step	0.018 , 5 , 10 , 20 , 30 , 40 , 50 ,51.58
Load Steps	0.018-5-10-20-30-40-50-51.58
Piecewise Steps	0.018-2-5
	5-10-20
	20-30-40
	40-50-51.8

3.5 Numerical methods used during application of loads

Three distinct numerical methods were used to apply loads on FE models: (1) single step, (2) multiple load steps and (3) piecewise steps. A step corresponds to single analyses. Table 3 presents the details of the analyses conducted in the present work.

In single step method, 8 different pressure loads were separately applied on the two finite element models FE-1 and FE-2. They were selected based on compression test: 0.018, 5, 10, 20, 30, 40, 50 and 51.58 MPa. 0.018 MPa was selected as the unloaded state of the specimens. The ultimate load of the samples was 51.58 MPa. Each load corresponded to a single static analysis. By default, the program automatically assigned time=1 at the end of each load in single step method. These pressures were applied at the nodes located on top area of the model, at location *Y*=0.075 m. A total of 8 piezoresistive static analyses were separately conducted.

In load steps method, 8 load steps were defined and solved sequentially in a single piezoresistive static analysis. The first load step corresponded to 0.018MPa (specimens' unloaded state), while the last load step corresponded to 51.58 MPa. The analysis was conducted on the two finite element models FE-1and FE-2. In this method, time can be assigned by the user at the end of each load step as a tracking parameter, so that the applied loads may vary incrementally over the 8 load steps. In this case, the first load step corresponding to 0.018 MPa pressure load ended at time=1, then the second load step corresponding to 5 MPa proceeded until time=2, and so on. A total of 8 load steps were gradually achieved within a single static analysis with the last load step equal to 51.58 MPa.

In piecewise steps method, 4 different static analyses were performed separately. 3 load steps were defined in each analysis. The last load step of a static analysis corresponded to the first load step of the subsequent analysis. Time was assigned by the user at the end of each load step, so that the applied loads may vary incrementally over the 3 load steps of the same analysis.

3.6 Evaluation of the numerical results

In order to compute the electrical resistivity of the model, two different ways can be followed. In the first way, the electric field and the current density (defined as the current I per unit cross-sectional area A) at different loads were determined from the analysis by element solution. In this case, the electrical resistivity ρ_m of the FE model at different applied loads was calculated using Eq. (6),

$$\rho_m = E / J \tag{6}$$

in which E denotes the output electric field vector sum (V/m) by element solution and J is the output current density vector sum (A/m^2) by element solution (Chung 2010, Mason and Thurston 1957, Mohammed *et al*. 2008).

In the second way, the electrical resistance at each point of the analysis was computed using Ohm's law as in Eq. (2), where $Rs=R$ is the electrical resistance of the model, $Vs=V$ the output potential difference obtained from the coupled inner voltage nodes of the model and Ic=I is the output current obtained by element solution. Eq. (1) can be rewritten as in Eq. (7).

$$R = V / I \tag{7}$$

In this case, the electrical resistivity ρ_e of the finite element model at each point of the analysis was evaluated by taking into account the length and cross sectional area of the model as in Eq. (2), where R is the electrical resistance of the model (Ω), L the length between inner electrodes (m) and A is the cross-section area of the model (m^2). Eq. (2) can be rewritten for the model as in Eq. (8).

$$\rho_e = R \times A / L \tag{8}$$

In all the cases, the electrical resistivity percent change of FE model was computed in virtue of Eq. (3). The output strain at each pressure load was also retrieved from the analysis. The FE results were compared with experimental results.

4. Results and discussions

In order to eliminate the polarization effects, 20 V DC current was supplied to the samples until steady state electrical resistance was obtained before the compression tests. A typical electrical resistance-time graph during polarization was presented in Fig. 6(a). The electrical resistance reached a steady state value at approximately 15 minutes of polarization as seen in Fig. 6(a).

The electrical resistivity percent change (% ρ) and compressive strain (ε) obtained from compression test on the 2 specimens are presented in Fig. 6(b). The % ρ, plotted on the vertical axis, took negative values which means that the electrical resistivity of the samples decreased during the test. The slope of the percent change in resistivity versus strain curve illustrates the strain sensitivity of a specimen multiplied by 100. As the slope increases, the sensitivity of smart concrete to applied strain increases. The correlation coefficient of best fit line for the two specimens was very close to 1, which testifies the strong relationship between the strain and % ρ. Mechanisms of piezoresistivity are filler reorientation which led to change in conductive networks; strain induced changes in volume and change of distance between conductive particles (García-Macías *et al*. 2018a). The decrease of electrical resistivity, thus piezoresistivity, was due to compressive strain, which led to closure of micro-cracks and micro-voids and increased the fiber-

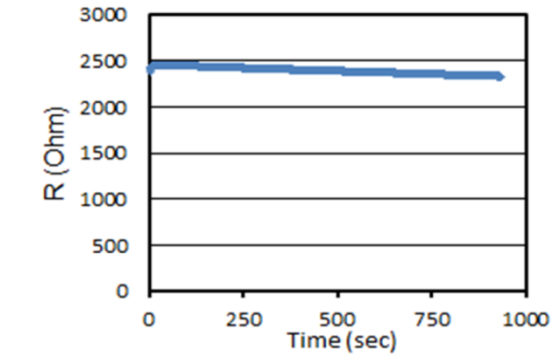

(a)

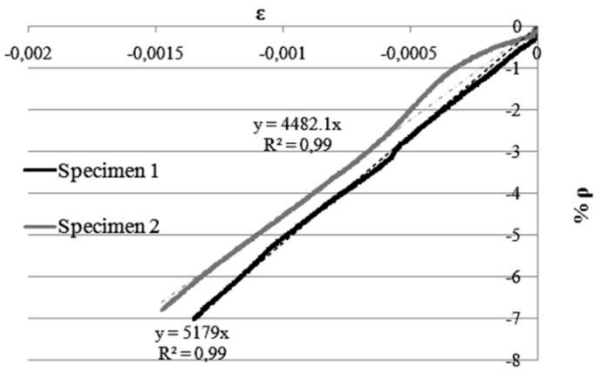

(b)

Fig. 6 (a) Electrical resistance-time graph during polarization with 20 V DC (b) The compression test, % ρ - compressive strain graph for Specimens 1 and 2

Table 4 The decrease of electrical resistivity (%) obtained from experimental results and FE models using single step, load steps and piecewise steps methods

Electrical Resistivity Decrease (%)					
FE Model	Single Step Method Using		Load Steps Method	Piecewise Steps Method	Experimental Results
	Equation 6 (E/J Model)	Equation 7 (V/I Model)			
FE-1	7	6.9	7	7	7
FE-2	6	6	6	6	6.8

matrix and fiber-fiber contact, enhancing electron transfer.

Table 4 presents the percentage decrease of electrical resistivity obtained in experiments as well as in numerical models using single step, load steps and piecewise steps methods. The percent decrease of electrical resistivity obtained from all the methods and experimental work were in compliance.

Figs. 7(a) and (b) respectively depict the electric field contour plots obtained in FE-1 model for the minimum (0.018 MPa) and maximum (51.58 MPa) pressure loads using single step method. Similarly, Figs. 7(c) and (d) present current density contour plots obtained in FE-1 model for the minimum (0.018 MPa) and maximum (51.58 MPa) pressure loads using single step method. When the pressure increased from minimum to maximum, the electric field decreased from 283.636 V/m to 278.182 V/m, while

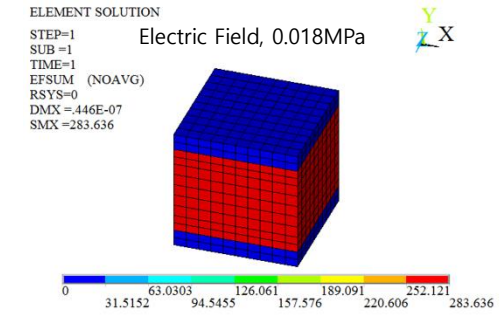

(a)

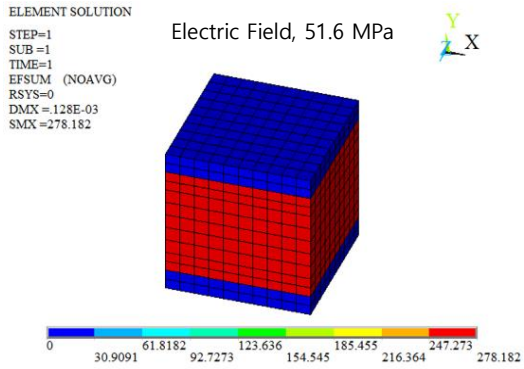

(b)

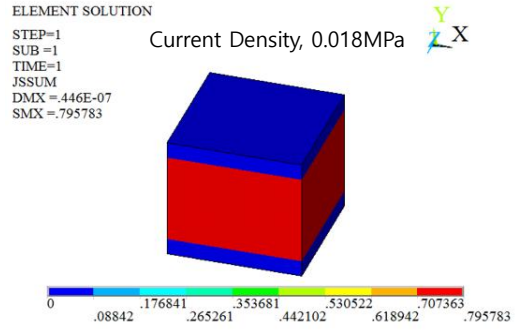

(c)

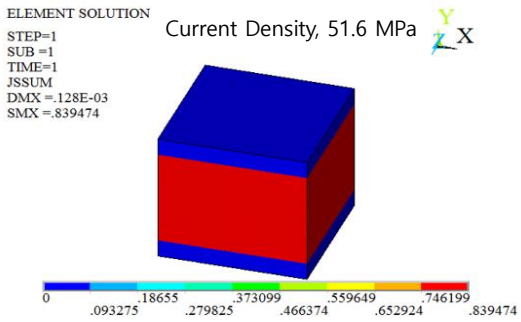

(d)

Fig. 7 Numerical contour plots of electric field vector sum (a) for the minimum (0.018 MPa) pressure load (b) for the maximum (51.58 MPa) pressure load (c) current density vector sum for the minimum (0.018 MPa) and (d) maximum (51.58 MPa) pressure loads of FE-1 model

the current density increased from 0.795783 A/m^2 to 0.839474 A/m^2. In all the models and methods used, the electric field decreased with applied strain, while the

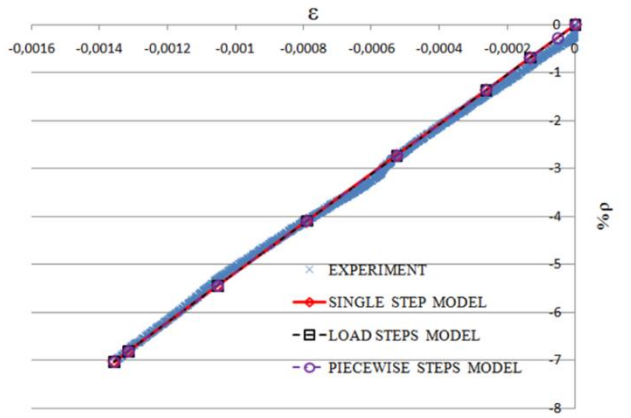

Fig. 8 Experimental and FEM % ρ - strain graphs using single, load steps and piecewise steps method; smart concrete specimen 1 vs FE-1 model

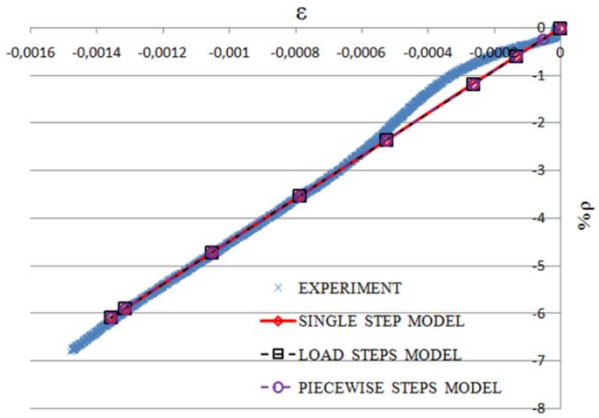

Fig. 9 Experimental and FEM % ρ - strain graphs using single, load steps and piecewise steps method; smart concrete specimen 2 vs FE-2 model

current density increased, resulting in a drop of electrical resistivity. Thus, the model was capable of simulating the piezoresistive behaviour.

Table 4 also shows that in single step method, the percent decrease of electrical resistivity obtained by using Eq. (6) (E/J model) and Eq. (7) (V/I model) are close to each other, which demonstrate the accuracy of the model and analyses.

The experimental results are plotted with the numerical results obtained from all the models using single step, load steps and piecewise steps methods in Figs. 8 and 9. On the numerical model curves, there are 8 points corresponding to applied loads in finite element modeling. The change in electrical resistivity (% ρ) in all numerical models linearly decreased with the applied strain (ε), which was also seen in experimental results. The maximum compressive strain obtained in the finite element models was approximately equal to the ultimate compressive strain obtained from experiments, regardless of the method used during solution. Thus, the Figs. 8 and 9 satisfactorily demonstrate the accuracy of the model.

In general, the resistivity change % ρ - strain plots from all the methods are in compliance with the experimental data.

5. Conclusions

The strain-electrical resistivity relation of smart concrete was modeled numerically. Piezoresistive static analysis was successfully conducted on two numerical models using finite element method. The finite element models were constructed using twenty-noded solid brick elements SOLID226 to simulate smart concrete specimens. The material properties were obtained from experimental data obtained from compression test. The smart concrete cube specimens were modeled as volumes with 75×75×75 mm dimensions.

The electrical resistivity was evaluated by following two different ways. In the first way, the electric field and the current density were computed from the models by element solution. The electrical resistivity of FE models was then calculated by dividing the electric field vector sum to the current density vector sum. In the second way, the electric potential difference and the current were determined from the models and the electrical resistance was calculated using Ohm's law. The electrical resistivity of numerical models was calculated by taking into account the length and cross sectional area of the models.

Finite element solution was conducted by using three different methods. Single step method was used to separately apply 8 static pressure loads on FE models in 8 static analyses. Load steps method helped to apply 8 time-dependent loads in a single static analysis. The loads were assumed to vary slowly with respect to time. Piecewise steps method served to conduct 4 static analyses with 3 time-dependent loads in each analysis. The numerical contour plots of electric field and current density by element solution for the lowest and highest pressure level obtained from the three methods were examined and discussed. The electrical resistivity change % ρ - strain graph obtained from finite element analysis was compared to the experimental results. The information and results gathered within the scope of this study are as follows:

- The simulation of piezoresistive behavior of smart concrete by finite element method was successfully conducted in this study. The FE model results comply with experimental results.
- The maximum compressive strain obtained in the finite element models was very close to the ultimate compressive strain obtained from experiments, regardless of the method used during solution.
- The electrical resistivity of the models decreased from the lowest to the highest pressure load, regardless of the method used during solution. The decrease of electrical resistivity was also observed in experiments. The compressive strain decreased the electrical resistivity with closure of micro-voids, resulting in increase of fiber-matrix and fiber-fiber contact, leading to piezoresistive behavior.
- Similar results were obtained from the evaluation of electrical resistivity through the use of electric field and current density and the use of Ohm's law.

The similarity between finite element results and

experimental findings indicates that the proposed numerical model is able to predict the piezoresistive behavior of smart concrete. Modeling of smart concrete will enable the creation of reliable finite element models that can be used by structural engineers to predict the strain-sensing capability of smart concrete for structural health monitoring.

Acknowledgements

This work was supported by The Scientific and Technological Research Council of Turkey (TUBITAK) through Grant no: 213M452 with project entitled "Smart Concrete Production". The author would like to thank to Batıçim and Batıbeton Co. for supplying the aggregates and cement; to Sika Construction Chemicals Co. for providing superplasticizer, to BASF Co. for supplying silica fume, to BMS Metal Co. for supplying brass fibers.

References

ANSYS Inc. (2011), ANSYS Help, Coupled-field analysis guide, ANSYS, https://www.sharcnet.ca/Software/Fluent14/help/ans_elem/Hlp _E_SOLID226.html.

Azhari, F. and Banthia, N. (2017), "Carbon fiber-reinforced cementitious composites for tensile strain sensing", *ACI Mater. J.*, **114**(1), 129-136.

Baeza, F.J., Zornoza, E., Andión, L.G., Ivorra, S. and Garcés, P. (2011), "Variables affecting strain sensing function in cementitious composites with carbon fibers", *Comput. Concrete*, **8**(2), 229-241. https://doi.org/10.12989/cac.2011.8.2.229.

Chen, B. and Liu, J. (2008), "Damage in carbon fiber-reinforced concrete, monitored by both electrical resistance measurement and acoustic emission analysis", *Constr. Build. Mater.*, **22**(11), 2196-2201. https://doi.org/10.1016/j.conbuildmat.2007.08.004.

Chen, P.W. and Chung, D.D.L. (1993), "Carbon fiber reinforced concrete for smart structures capable of non-destructive flaw detection", *Smart Mater. Struct.*, **2**(1), 22-30. https://doi.org/10.1088/0964-1726/2/1/004.

Chiarello, M. and Zinno, R. (2005), "Electrical conductivity of self monitoring CFRC", *Cement Concrete Compos.*, **27**, 463-469. https://doi.org/10.1016/j.cemconcomp.2004.09.001.

Chowdhury, S. (2017), "Experimental investigations and modeling of the strain sensing response of matrices containing metallic inclusions", MSc Dissertation, Arizona State University, Arizona, USA.

Chung, D.D.L. (2001), "Review functional properties of cement-matrix composites", *J. Mater. Sci.*, **36**(6), 1315-1324. https://doi.org/10.1023/A:1017522616006.

Chung, D.D.L. (2002), "Piezoresistive cement-based materials for strain sensing", *J. Intel. Mater. Syst. Struct.*, **13**(9), 599-609. https://doi.org/10.1106/104538902031861.

Chung, D.D.L. (2010), *Electrical Properties of Composite Materials*, 2nd Edition, Springer, New York, USA.

Fu, X. and Chung, D.D.L. (1997), "Effect of curing age on the self-monitoring behavior of carbon fiber reinforced mortar", *Cement Concrete Res.*, **27**(9), 1313-1318. https://doi.org/10.1016/S0008-8846(97)00118-X.

Fu, X., Chung, D.D.L., Ma, E. and Anderson, W.A. (1997), "Self-monitoring in carbon fiber reinforced mortar by reactance measurement", *Cement Concrete Res.*, **27**(6), 845-852. https://doi.org/10.1016/S0008-8846(97)83277-2.

García-Macías, E. and Ubertini, F. (2019), "Earthquake-induced damage detection and localization in masonry structures using smart bricks and Kriging strain reconstruction: A numerical study", *Earthq. Eng. Struct. Dyn.*, **48**(5), 548-569. https://doi.org/10.1002/eqe.3148.

García-Macías, E., Castro-Triguero, R., Sáez, A. and Ubertini, F. (2018a), "3D mixed micromechanics-FEM modeling of piezoresistive carbon nanotube smart concrete", *Comput. Meth. Appl. Mech. Eng.*, **340**, 396-423. https://doi.org/10.1016/j.cma.2018.05.037.

García-Macías, E., D'Alessandro, A., Castro-Triguero, R., Pérez-Mira, D. and Ubertini, F. (2017), "Micromechanics modeling of the electrical conductivity of carbon nanotube cement-matrix composites", *Compos. Part B: Eng.*, **108**, 451-469. https://doi.org/10.1016/j.compositesb.2016.10.025.

García-Macías, E., Rodríguez-Tembleque, L. and Sáez, A. (2018c), "MWCNT/epoxy strip-like sensors for buckling detection in beam-like structures", *Thin Wall. Struct.*, **133**, 27-41. https://doi.org/10.1016/j.tws.2018.09.013.

García-Macías, E., Rodríguez-Tembleque, L., Sáez, A. and Ubertini, F. (2018b), "Crack detection and localization in RC beams through smart MWCNT/epoxy strip-like strain sensors", *Smart Mater. Struct.*, **27**, 115022. https://doi.org/10.1088/1361-665X/aae668.

Han, B., Guan, X. and Ou, J. (2007), "Electrode design, measuring method and data acquisition system of carbon fiber cement paste piezoresistive sensors", *Sensor. Actuat.: A- Phys.*, **135**(2), 360-369. https://doi.org/10.1016/j.sna.2006.08.003.

Han, B.G., Sun, S.W. and Ding, S.Q. (2015), "Review of nanocarbon-engineered multifunctional cementitious composites", *Compos. Part A: Appl. Sci. Manuf.*, **70**, 69-81. https://doi.org/10.1016/j.compositesa.2014.12.002.

Kamila, S. (2013), "Introduction, classification and applications of smart materials: an overview", *Am. J. Appl. Sci.*, **10**(8), 876-880. https://doi.org/10.3844/ajassp.2013.876.880.

Li, H., Xiao, H. and Ou, J. (2006), "Effect of compressive strain on electrical resistivity of carbon black-filled cement -based composites", *Cement Concrete Compos.*, **28**(9), 824-828. https://doi.org/10.1016/j.cemconcomp.2006.05.004.

Li, H., Xiao, H. and Ou, J. (2008), "Electrical property of cement-based composites filled with carbon black under long-term wet and loading condition", *Comput Sci. Tech.*, **68**(9), 2114-2119. https://doi.org/10.1016/j.compscitech.2008.03.007.

Madenci, E. and Güven, I. (2006), *The Finite Element Method And Applications In Engineering Using ANSYS*, 1st Edition, Springer, New York, USA.

Mason, W.P. and Thurston, R.N. (1957), "Use of piezoresistive materials in the measurement of displacement, force, and torque", *J. Acoust. Soc. Am.*, **29**(10), 1096-1101. https://doi.org/10.1121/1.1908710.

Mohammed, A.A.S., Moussa, W.A. and Lou, E. (2008), "High sensitivity MEMS strain sensor: design and simulation", *Sensor.*, **8**(4), 2642-2661. https://doi.org/10.3390/s8042642.

Reza, F., Batson, G.B., Yamamuro, J.A. and Lee, J.S. (2003), "Resistance changes during compression of carbon fiber cement composites", *J. Mater. Civil Eng.*, **15**(5), 476-483. https://doi.org/10.1061/(ASCE)0899-1561(2003)15:5(476).

Teomete, E. (2014), "Transverse strain sensitivity of steel fiber reinforced cement composites tested by compression and split tensile tests", *Constr. Build. Mater.*, **55**, 136-145. https://doi.org/10.1016/j.conbuildmat.2014.01.016.

Teomete, E. (2015), "Measurement of crack length sensitivity and strain gage factor of carbon fiber reinforced cement matrix composites", *Measur.*, **74**, 21-30. https://doi.org/10.1016/j.measurement.2015.07.021.

Teomete, E. (2016), "The effect of temperature and moisture on electrical resistance, strain sensitivity and crack sensitivity of

steel fiber reinforced smart cement composite", *Smart Mater. Struct.*, **25**, 075024. https://doi.org/10.1088/0964-1726/25/7/075024.

Teomete, E. (2017), "Crack length and tensile strain correlation with electrical resistance of carbon fiber reinforced cement matrix composites measured by three-point bending test and splitting tensile test", *Cement Wapno Beton*, **22**(1), 3-19.

Teomete, E. and Koçyiğit, O.I. (2013), "Tensile strain sensitivity of steel fiber reinforced cement matrix composites tested by split tensile test", *Constr. Build. Mater.*, **47**, 962-968. https://doi.org/10.1016/j.conbuildmat.2013.05.095.

Teomete, E. and Koçyiğit, O.I. (2015), "Correlation between compressive strain and electrical resistance in carbon fiber reinforced cement composites", *Cement Wapno Beton*, **1**, 1-10.

Wang, H., Gao, X. and Liu, J. (2018a), "Coupling effect of salt freeze-thaw cycles and cyclic loading on performance degradation of carbon nanofiber mortar", *Cold Reg. Sci. Technol.*, **154**, 95-102. https://doi.org/10.1016/j.coldregions.2018.07.002.

Wang, Y., Wang, Y., Wan, B., Han, B., Cai, G. and Chang, R. (2018b), "Strain and damage self-sensing of basalt fiber reinforced polymer laminates fabricated with carbon nanofibers/epoxy composites under tension", *Compos. Part A: Appl. Sci. Manuf.*, **113**, 40-52. https://doi.org/10.1016/j.compositesa.2018.07.017.

Wang, Y., Wang, Y., Wan, B., Han, B., Cai, G. and Li, Z. (2018c), "Properties and mechanisms of self-sensing carbon nanofibers/epoxy composites for structural health monitoring", *Compos. Struct.*, **200**, 669-678. https://doi.org/10.1016/j.compstruct.2018.05.151.

Wen, S. and Chung, D.D.L. (2006), "Model of piezoresistivity in carbon fiber cement", *Cement Concrete Res.*, **36**(10), 1879-1885. https://doi.org/10.1016/j.cemconres.2006.03.029.

Wen, S. and Chung, D.DL. (2000), "Uniaxial tension in carbon fiber reinforced cement, sensed by electrical resistivity measurement in longitudinal and transverse directions", *Cement Concrete Res.*, **30**(8), 1289-1294. https://doi.org/10.1016/S0008-8846(00)00304-5.

Xiao, H., Li, H. and Ou, J. (2010), "Modeling of piezoresistivity of carbon black filled cement-based composites under multi-axial strain", *Sensor. Actuat.: A- Phys.*, **160**(1), 87-93. https://doi.org/10.1016/j.sna.2010.04.027.

HK